A Study on Friction Dampers and Their Contact Geometry Design

Jimmy Aramendiz and Alexander Fidlin

1 Introduction

Effective, targeted vibration damping with low efficiency reduction is an important goal for a modern design, especially for lightweight constructions and energy-efficient applications. An ideal damper dissipates energy only near the resonance frequency, when the undesired vibration amplitudes jeopardize the service life or function of the system. Such dampers increase the overall energy efficiency of a system.

To suppress undesired vibrations, viscous damping is introduced into the system in most applications, e.g. in the automotive industry in the form of a hydraulic shock absorber [2]. These damping mechanisms are always active and constantly dissipate energy even when this is not necessary. Thus, reducing the energy efficiency of the system. However, viscous damping is not the only way to reduce vibrations. The use of absorbers for vibration reduction is also common in engineering [1, 11]. Vibration absorbers achieve at their tuned operating frequency optimal vibration reduction. Nevertheless, at least one structural resonance must be overcome to reach the operating frequency. Furthermore, these devices are sensitive to the inevitable system parameter changes due to wear, time, and environmental conditions.

An additional alternative in vibration reduction are friction-based dampers, which are widely used in engineering. These dampers are used mainly in three different fields: in turbomachinery as so-called platform dampers, in civil engineering structures such as buildings and cables, and in railroad freight trucks. Platform dampers are in most cases metal elements which are pressed between two blade platforms by the centrifugal force in a gas turbine. These dampers are investigated mainly in

J. Aramendiz (✉) · A. Fidlin
Karlsruhe Institute of Technology, Kaiserstraße 10, 76131 Karlsruhe, Germany
e-mail: jimmy.aramendiz@kit.edu

A. Fidlin
e-mail: alexander.fidlin@kit.edu

P. Eberhard (ed.), *Calm, Smooth and Smart*, Lecture Notes in Applied and Computational Mechanics 102, https://doi.org/10.1007/978-3-031-36143-2_2

two variations: as curved friction dampers and as wedge (or cottage-roof) friction dampers [10]. In civil engineering friction dampers are mainly found in two forms. In some applications, planar contact surfaces are combined, whereas in other applications varying contact geometries are used. Applications with planar contact surfaces are found in [13], whereas investigations with geometric variations are presented in [9]. A special variant of friction dampers, the so called wedge dampers, are used in railroad trucks. These dampers are composed of a wedge placed between the bolster, which carries the wagon, and side frame, which is connected to the wheels. The geometric variations in the dampers' sliding contact partners "simulate" a viscous damping avoiding technological difficulties connected with the handling of fluids. Due to their robustness, low cost, and low maintenance they are quite popular and still investigated today [14].

A possible passive implementation of an energy-efficient vibration suppression can be realized by dry friction. The special character of dry friction with stick-slip transitions allows the design of elements that change their behavior. Frictional contacts, which can stick and slide, change the structure of a system and thus its behavior. The targeted design of the sticking and sliding dynamics allows systems to passively adapt to current operating conditions. This paper focuses on three such passive dry friction dampers: the dry friction lock-up damper, a prestressed sliding wedge damper, and the friction damper with polynomial contact geometry. The underlying operating principle of the dampers is based on the stick-slip properties of dry friction. This ensures sticking at low excitation amplitudes, which prevents any relative movement between the masses and thus no energy is dissipated. As soon as the breakaway force of the damper is overcome, the system moves in the stick-slip range. The breakaway condition ensures a selective energy dissipation, which only occurs at high vibration amplitudes. This work uses the simplest friction model namely the Coulomb model, in which Stribeck effects and a difference between static and dynamic friction coefficients are neglected.

The present paper is structured as follows. In Sect. 2 the dry friction lock-up damper is investigated. The equations of motion of the dampers are derived and numerical parameter studies are performed, which gives a first impression of the system dynamics. In addition, an analytical solution for the systems is derived and analyzed using the averaging method. Analogous investigations are carried out in Sect. 3. Analytical solutions for different polynomial degrees are derived in Sect. 4 for the dry friction damper with polynomial contact surface. Experimental results are presented in Sect. 5. The main findings are summarized in Sect. 6.

2 The Dry Friction Lock-Up Damper

The goal of the dry friction lock-up damper (Fig. 1) is to improve the dynamics of an existing main system. In this paper the main system is represented by the primary spring c_1 and the primary mass m_1. The lock-up damper, consisting of a dry friction element with friction force R, a secondary spring c_2, and a secondary mass m_2 is

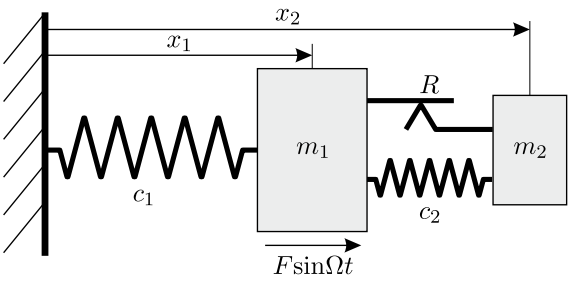

Fig. 1 Lock-up with a harmonic excitation on the primary mass

attached to the main system. Due to the neglecting of both Stribeck effects and a difference between static and sliding friction coefficients, the friction force R also corresponds to the breakaway force of the friction element. The friction element determines the stick-slip behavior of the system and thus also the conditions under which the secondary spring influences the system dynamics. While sticking both masses move together in the same way and the secondary spring is inactive. In the inactive state, the secondary spring can be in a deflected state, but this does not affect the motion of the system. The inactive secondary spring only affects the stiction force. As soon as the friction element allows relative movement, the structure of the system changes from a one degree to a two degrees of freedom oscillator. This leads to a change in the number and value of of the system's natural frequencies. The stick-slip properties divide the system behavior into linear and nonlinear ranges, each of which is determined by the closed and open state of the friction element respectively. Therefore the system's dynamics are characterized by these two ranges: the sticking range and the sliding range. The system is in the sticking range as long as the absolute value of the stiction force H is smaller than the breakaway force R ($|H| \leq R$) and the kinematic condition $\dot{x}_1 = \dot{x}_2$ is fulfilled. If one of these conditions is violated, the system switches to the sliding range. The equations of motion for both ranges are given by

while sticking

$$(m_1 + m_2)\ddot{x}_1 + c_1 x_1 = F \sin \Omega t, \tag{1}$$

$$H = m_2\ddot{x}_2 + c_2(x_2 - x_1), \tag{2}$$

while sliding

$$m_1\ddot{x}_1 + c_1 x_1 - c_2(x_2 - x_1) - R\,\mathrm{sgn}(\dot{x}_2 - \dot{x}_1) = F \sin \Omega t, \tag{3}$$

$$m_2\ddot{x}_2 + c_2(x_2 - x_1) + R\,\mathrm{sgn}(\dot{x}_2 - \dot{x}_1) = 0. \tag{4}$$

The sticking range is described by one equation of motion and one algebraic equation for the stiction force, whereas the sliding range is characterized by two equations of motion. As described in [5], it is intuitive that the amplitude response of the whole system follows the amplitude response of the linear system up to a certain breakaway amplitude. After the breakaway point, a nonlinear region follows, where

stick-slip and full sliding movements occur. The nonlinear range is only concluded by the complete closing of the friction point over an entire period. Afterwards, the amplitude response of the entire system follows the amplitude response of the linear system with one degree of freedom again.

2.1 Numerical Investigations

To gain a first insight into the dynamics of the lock-up damper, numerical parameter studies are carried out. The parameters of the main system are usually determined a priori and therefore cannot be modified. In these studies, both the mass and the spring stiffness are set to one without any restriction of the generality. Since the total mass of the system should not be significantly changed, the value of the secondary mass is chosen to be much smaller than the primary mass, e.g. one tenth of the primary mass. In order to reduce amplitudes over the entire frequency spectrum, the secondary stiffness is chosen to cancel out the resonance of the main system. Only the breakaway force of the friction element remains as a freely selectable design parameter. A parameter study on the influence of the friction force [12] is shown in Fig. 2 for the parameters

$$m_1 = 1\,\text{kg},\ m_2 = 0.1\,\text{kg},\ c_1 = 1\,\text{N/m},\ c_2 = 0.1\,\text{N/m},\ F = F_0 = 0.1\,\text{N}.$$

The friction force R determines the breakaway frequency and thus determines whether the system behaves mainly like a one or two degrees of freedom system. For a system with one peak it is necessary that the breakaway frequency is higher than the first resonance frequency of the two degrees of freedom system. On the basis of this

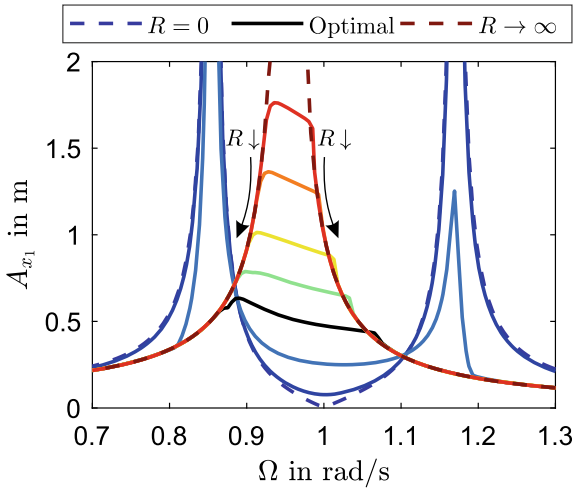

Fig. 2 Parameter study of the lock-up damper for $R \in$ [0N(blau), 1.5N(rot)], $R_{\text{opt}} \approx 0.0369$ N

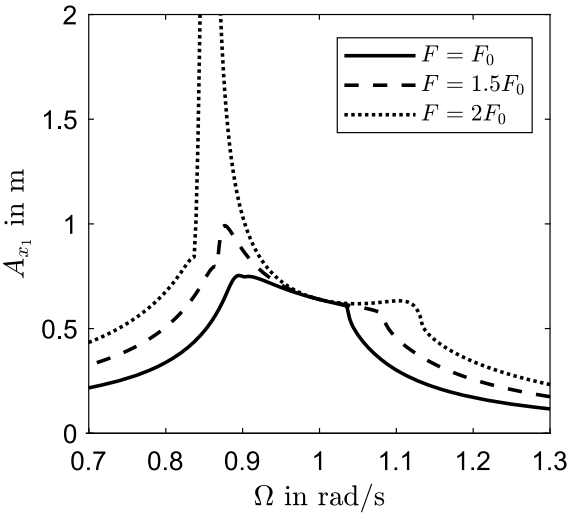

Fig. 3 Parameter study of the lock-up damper for different excitation forces with $R = 0.05$ N

parameter study the existence of an optimal friction force is identified. The optimal friction force leads to a minimization of the maximum amplitude in the frequency spectrum and must be tuned to the excitation force. This is clearly shown in Fig. 3. An increase of the excitation force with the same friction force leads to considerably larger amplitudes in a detuned lock-up damper. The reason for this is the relationship between the energy dissipated by the damper and the relative amplitude. The friction force is constant over the displacement. This leads to an energy dissipation proportional to the relative amplitude. In the detuned case the dissipated energy is not sufficient to limit the amplitudes. With the selected parameters, this effect can be seen when the excitation is doubled.

2.2 Analytical Investigations

After the insight into the dynamics of the lock-up damper, an analytical solution is advantageous for a deeper understanding of the system. A detailed description of this solution can be found in [6]. To derive an analytical solution for this system, the nonlinear equations of the system are considered. It is additionally assumed that permanent sliding occurs. The first step is to derive the nondimensional equations of motion of the system. The necessary transformations are

$$z_1 = \frac{m_1 x_1 + m_2 x_2}{m_1 + m_2},\ z_2 = x_2 - x_1, \tag{5}$$

$$\varepsilon = \frac{m_2}{m_1 + m_2} \ll 1,\ k = \sqrt{\frac{c_1}{m_1}},\ \lambda = \sqrt{\frac{c_2}{m_2}},\ p = \frac{\lambda}{k}, \tag{6}$$

$$\tau = kt,\ (\cdot)' = \frac{\mathrm{d}}{\mathrm{d}\tau}(\cdot),\ \eta = \frac{\Omega}{k},\ \mu = \frac{R}{m_2 k^2 (1-\varepsilon)}, \tag{7}$$

$$f_0 = \frac{F}{k^2(m_1 + m_2)} = \varepsilon f,\ f = \mathcal{O}(1). \tag{8}$$

The newly introduced variables z_1 and z_2 represent the movement of the center of mass of the entire system and the relative movement between the masses. These transformations lead to the nondimensional equations

$$z_1'' + z_1 = \varepsilon(z_1 + z_2 + f \sin \eta\tau) - \varepsilon^2 z_2, \tag{9}$$

$$z_2'' + \frac{p^2}{1-\varepsilon} z_2 + \mu \mathrm{sgn}(z_2') = z_1 - \varepsilon \left(z_2 + \frac{f}{1-\varepsilon} \sin \eta\tau \right). \tag{10}$$

In order to obtain suitable equations for the averaging procedure, a Van der Pol transformation is additionally applied and the slowly changing amplitudes and phase differences of the variables are considered. This yields

$$z_1 = A \sin \varphi,\ z_1' = A \cos \varphi, \tag{11}$$

$$z_2 = B \sin \psi,\ z_2' = Bp \cos \psi, \tag{12}$$

$$\gamma = \varphi - \eta\tau,\ \varepsilon\delta_1 = 1 - \eta, \tag{13}$$

$$\theta = \psi - \varphi,\ \varepsilon\delta_2 = p - \eta, \tag{14}$$

$$A' = \varepsilon(f \sin \eta\tau + A \sin \varphi + B \sin \psi) \cos \varphi - \varepsilon^2 B \sin \psi \cos \varphi, \tag{15}$$

$$\gamma' = \varepsilon\delta_1 - \varepsilon(f \sin \eta\tau + A \sin \varphi + B \sin \psi) \sin \varphi + \varepsilon^2 B \sin \psi \sin \varphi, \tag{16}$$

$$\begin{aligned} B' = {} & \frac{\varepsilon}{p} \left((\tilde{A} \sin \varphi - \tilde{\mu} \mathrm{sgn}(\cos \psi) - (1 + p^2) B \sin \psi \right) \cos \psi \\ & - \frac{\varepsilon^2}{p} \left(p^2 B \sin \psi + \tilde{f} \sin \eta\tau \right) \cos \psi, \end{aligned} \tag{17}$$

$$\begin{aligned} \theta' = {} & \varepsilon\delta_2 + \frac{\varepsilon}{p} \left(\tilde{\mu} \mathrm{sgn}(\cos \psi) + (1 + p^2) B \sin \psi \right) \sin \psi \\ & - \frac{\varepsilon}{p} \tilde{A} \sin \varphi \sin \psi + \frac{\varepsilon^2}{p} \left(p^2 B \sin \psi + \tilde{f} \sin \eta\tau \right) \sin \psi. \end{aligned} \tag{18}$$

It should be noted that in the Eqs. 17 and 18 the scaling $A = \varepsilon \tilde{A}$, $\mu = \varepsilon \tilde{\mu}$ and $f = \varepsilon \tilde{f}$ was applied. The reason for this, is that Eq. 10 depends only on the ratios of these quantities and not on the actual quantities themselves. If these selected parameters are scaled with the same factor, the equation will qualitatively yield the same solution scaled only by the selected factor. For a more detailed explanation, the reader is referred to [6]. If a first and second order averaging procedure is applied to

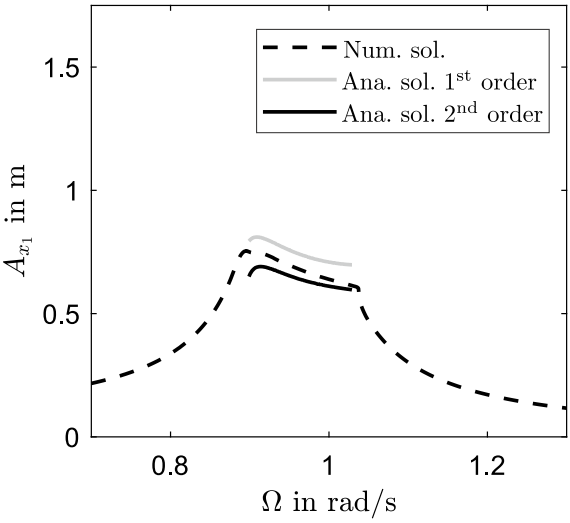

Fig. 4 Analytical solution of the lock-up damper

the Eqs. 15–18, the analytical solutions in Fig. 4 is obtained. The first-order solution represents the qualitative behavior of the amplitude response. The resonance peak of the system is limited and a declining characteristic curve in the resonance range can be observed. The second order solution provides a quantitative improvement of the result. It is also demonstrated, that the damper is very sensitive to changes of the excitation amplitude (or the changes of the friction coefficient). Therefore, its applicability is limited.

3 The Prestressed Sliding Wedge Damper

Similar to the lock-up damper, the aim of the prestressed sliding wedge damper is to improve the dynamics of a main system with spring stiffness c_1 and mass m_1. The damper is attached to the main system and consists of a prestressed mass m_2

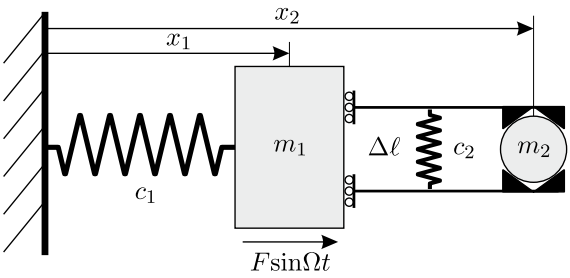

Fig. 5 The prestressed sliding wedge damper

between two wedges with the wedge angle α, see Fig. 5. The prestress force acting on the wedges is produced by a spring of stiffness c_2, which is prestressed by a length $\Delta\ell$. In addition, the coefficient of friction μ describes the relationship of the normal force to the friction force between the wedges and the mass. A relative movement of the masses presses the wedges apart symmetrically. Furthermore, the wedges are mounted on the main mass in such a way that they only transmit a force in the vibration direction. Because the wedges are pressed apart, this damper more robust compared to the lock-up damper. The friction force of the lock-up damper is constant, whereas the friction force in the prestressed sliding wedge damper depends on the relative displacement. If there is a relative displacement between the masses, the normal force between the wedges and the mass increases due to the geometry and spring deflection. This change ultimately leads to a variable friction force, which achieves limited vibration amplitudes at different excitation force amplitudes. Analytical investigations of this system without preload can be found in [4]. The industrial implementation of a sliding wedge damper without prestress in a drive train is described in [8] and is called a anti-clutch-judder-damper (germ.: Anti-Rupf-Tilger).

From a practical point of view, it makes sense to choose small coefficients of friction, because these lead to a longer service life of the damper [7]. However, a reduction of the coefficient of friction also reduces the energy dissipation. If this effect is not desired, compensation can be made by adjusting the angle α. The equations of motion of the system are given by

while sticking

$$(m_1 + m_2)\ddot{x}_1 + c_1 x_1 = F \sin \Omega t, \tag{19}$$

$$H = \frac{m_2}{m_1 + m_2}(F \sin \Omega t - c_1 x_1), \tag{20}$$

while sliding

$$m_1 \ddot{x}_1 + c_1 x_1 - F_{\mathrm{WD}} = F \sin \Omega t, \tag{21}$$

$$m_2 \ddot{x}_2 + F_{\mathrm{WD}} = 0, \tag{22}$$

$$F_{\mathrm{WD}} = 2c_2 \ (2 \tan \alpha |x_2 - x_1| + \Delta\ell) \frac{\tan \alpha \mathrm{sgn}(x_2 - x_1) + \mu \mathrm{sgn}(\dot{x}_2 - \dot{x}_1)}{1 - \mu \mathrm{sgn}(\dot{x}_2 - \dot{x}_1) \tan \alpha \mathrm{sgn}(x_2 - x_1)} \ . \tag{23}$$

The stiction force H in Eq. 20 represents the necessary constraining force to prevent relative movement between the primary and secondary mass. Accordingly, it is not the stiction force between the wedges and the mass m_2. Furthermore, for small coefficients of friction it is permissible to linearize the damper force with respect to the friction parameter. As shown in Fig. 6 the damper force can be broken down into a dissipation-free portion $F_{\mathrm{C,WD}}$ and a dissipativ portion $F_{\mathrm{D,WD}}$. These terms are described by

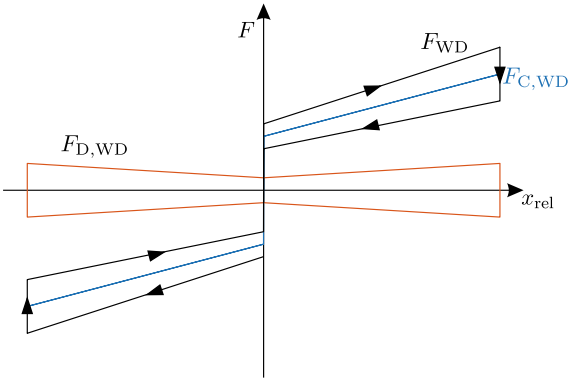

Fig. 6 Break down of the damper force of the prestressed sliding wedge damper with $x_{\mathrm{rel}} = x_2 - x_1$

$$F_{\mathrm{WD}} = F_{\mathrm{C,WD}} + F_{\mathrm{D,WD}}, \tag{24}$$

$$F_{\mathrm{C,WD}} = 2c_2(2\tan\alpha(x_2 - x_1) + \Delta\ell\,\mathrm{sgn}(x_2 - x_1))\tan\alpha, \tag{25}$$

$$F_{\mathrm{D,WD}} = 2c_2\,(2\tan\alpha|x_2 - x_1| + \Delta\ell)\,\frac{\mu}{\cos^2\alpha}\,\mathrm{sgn}(\dot{x}_2 - \dot{x}_1). \tag{26}$$

The nonlinearities in the wedge damper are much more pronounced than in the lock-up damper, because for this damper there are discontinuities in its force both as a function of the position and as a function of the velocity. In addition, the dissipative part of the damper force is proportional to the displacement. As a result, the dissipated energy is proportional to the square of the relative amplitude, similar to a viscous damper. Based on this finding, the authors of this work refer to this device as a pseudo-viscous damper.

3.1 Numerical Investigations

The first findings of this system are obtained by numerical simulations. As in Sect. 2, the parameters of the main system are exemplary set to one and the secondary mass is chosen as one tenth of the main mass. However, the prestresses sliding wedge damper offers a higher design flexibility, since the wedge angle α, the coefficient of friction μ, the preload length $\Delta\ell$ and the secondary stiffness c_2 can be considered as design parameters. The numerical studies of this work are limited to two design parameters α and $\Delta\ell$ and to the robustness of the system against the excitation amplitude F. Unless otherwise specified, the following standard parameters are used for the numerical studies

$$m_1 = 1\ \mathrm{kg},\ m_2 = 0.1\ \mathrm{kg},\ c_1 = 1\ \mathrm{N/m},\ c_2 = 0.1\ \mathrm{N/m},$$
$$F = F_0 = 0.01\ \mathrm{N},\ \alpha = 30^\circ,\ \Delta\ell = 0.01\ \mathrm{m},\ \mu = 0.01.$$

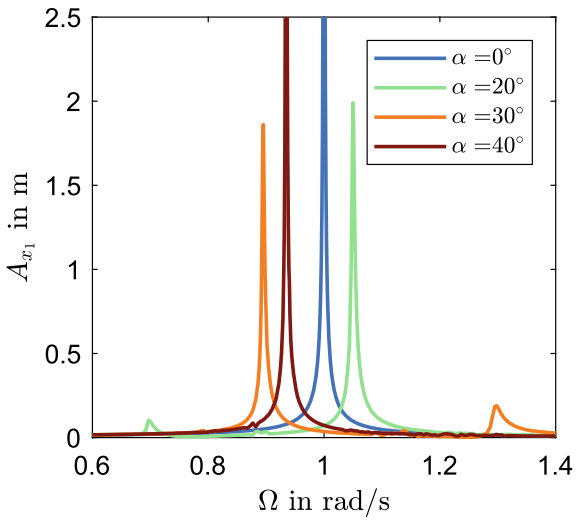

Fig. 7 Parameter study of the prestressed sliding wedge damper for different wedge angles α

The variation of the wedge angle α shows that this parameter has a significant influence on the effective stiffness $c_{2,\text{eff}}$ between the masses. Based on the non-dissipative part of the damper force, the effective stiffness can be derived as the coefficient of relative displacement, $c_{2,\text{eff}} = 4c_2 \tan^2 \alpha$, cf. Eq. 25. This influence is shown in Fig. 7. At small angles, there is a low effective stiffness and thus a peak at low frequencies and a peak near the resonance of the sticking system. Increasing the effective stiffness by the changing angle α causes both resonances to shift to the right, increasing the first peak and decreasing the second one. Additionally, the wedge angle has an influence on the dissipated energy. The higher the wedge angle, the higher the dissipative force at constant relative displacement, cf. Eq. 26.

Similar to the friction force of the lock-up damper, the prestress displacement determines the breakaway frequency at which the system changes to the nonlinear stick-slip range. The parameter study of the prestress displacement $\Delta\ell$ is shown in Fig. 8. A nonexistent prestress ($\Delta\ell = 0$) results in a two degrees of freedom system that does not stick. If the prestress displacement is increased, the sliding range is reduced and two sticking ranges appear at the edges of the amplitude response. The higher the displacement, the larger the sticking ranges become. For $\Delta\ell \to \infty$ the system always sticks. An optimum prestress displacement exists for this system as well. This optimum causes the best possible switching between the two extreme cases and thus achieves lower vibration amplitudes. Furthermore, non-periodic solutions can occur in the system. These can be both quasi-periodic and chaotic. For lowest possible vibration amplitudes over the whole frequency range, this type of solution should be avoided.

The last study of the friction absorber deals with the robustness of the system against a change of the excitation force amplitude. Figure 9 shows the normalized magnification factor of the system for different excitation forces. In contrast to the

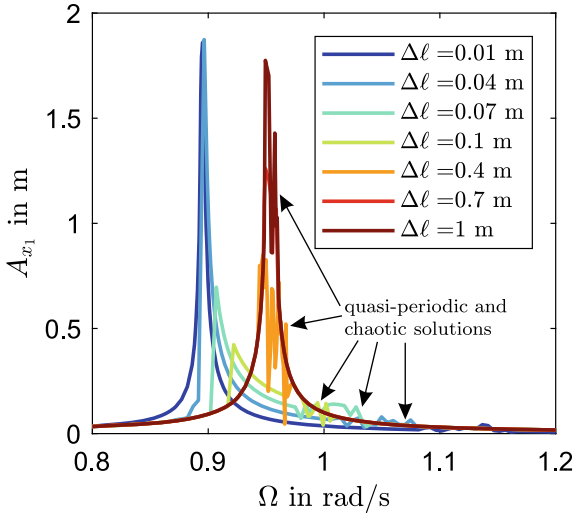

Fig. 8 Parameter study of the prestressed sliding wedge damper for different preload displacements $\Delta\ell$

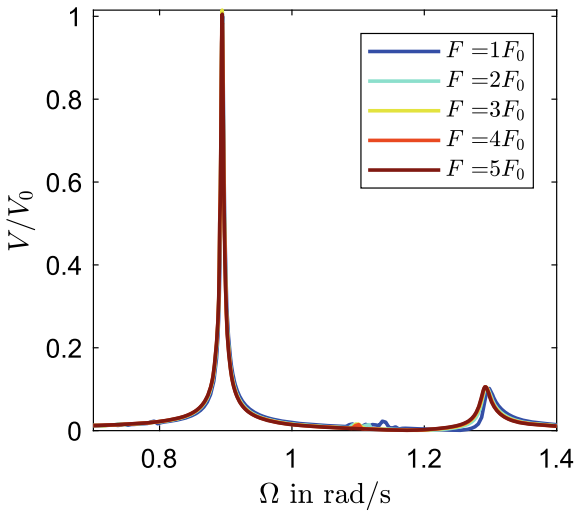

Fig. 9 Parameter study of the prestressed sliding wedge damper for different excitations forces F with $V = A_{x_1,F}/F,\ V_0 = A_{x_1,F_0}/F_0$

lock-up damper, the amplitudes remain limited. The curves are not directly on top of each other, but the differences are minimal. An increase of the excitation force causes almost no change of the magnification factor. Consequently, the vibration amplitudes of the system are amplified by approximately the same factor. This implies a scalability of the amplitude responses, although an exact scalability can only be observed in linear mechanical systems with viscous damping. These last correlations confirm the pseudo-viscous behavior of the friction damper.

3.2 Analytical Investigations

The analytical solution of the friction damper [4] is derived analogous to the lock-up damper via an averaging method. For this purpose the equations are nondimensionalized and the following dimensionless parameters are introduced

$$\lambda = \frac{m_2}{m_1},\ k^2 = \frac{c_1}{m_1},\ f = \frac{F}{m_1 k^2}, \tau = kt,\ (\cdot)' = \frac{\mathrm{d}}{\mathrm{d}\tau}(\cdot),\ \eta = \frac{\Omega}{k}, \tag{27}$$

$$a = \tan^2\alpha,\ b = \mu\frac{\tan\alpha}{\cos^2\alpha}c = \Delta\ell\tan\alpha,\ d = \frac{\Delta\ell\mu}{\cos^2\alpha}, \tag{28}$$

$$\varepsilon \ll 1, \qquad f,\ \Delta\ell,\ \mu = \mathcal{O}(\varepsilon). \tag{29}$$

If these dimensionless parameters are set in Eqs. 19–22, the dimensionless differential equations are given by

$$\begin{aligned} x_1'' + x_1 + 4\lambda a(x_1 - x_2) &= f\sin\eta\tau \\ &\quad -4\lambda b|x_1 - x_2|\mathrm{sgn}(x_1' - x_2') - 2\lambda c\,\mathrm{sgn}(x_1 - x_2), \end{aligned} \tag{30}$$

$$\lambda x_2'' - 4\lambda a(x_1 - x_2) = 4\lambda b|x_1 - x_2|\mathrm{sgn}(x_1' - x_2') + 2\lambda c\,\mathrm{sgn}(x_1 - x_2). \tag{31}$$

Equations 30 and 31 are rewritten in matrix form and a modal transformation is applied

$$\mathbf{M}\mathbf{x}'' + \mathbf{C}\mathbf{x} = \varepsilon\mathbf{f}_{NL}(\mathbf{x}, \Omega), \tag{32}$$

$$\mathbf{x} = \mathbf{R}\mathbf{z} = \mathbf{R}[p, q]^\top \text{ with } \mathbf{R}^\top\mathbf{M}\mathbf{R} = \mathbf{I},\ \mathbf{R}^\top\mathbf{C}\mathbf{R} = \mathrm{diag}(\eta_i^2), \tag{33}$$

$$\mathbf{R}^\top\mathbf{M}\mathbf{R}\mathbf{z}'' + \mathbf{R}^\top\mathbf{C}\mathbf{R}\mathbf{z} = \varepsilon\mathbf{R}^\top\mathbf{f}_{\mathrm{NL}}(\mathbf{z}) = \varepsilon\tilde{\mathbf{f}}_{\mathrm{NL}}(\mathbf{z}), \tag{34}$$

$$p'' + \eta_{01}^2 p = \varepsilon\tilde{f}_{\mathrm{NL},1}(p, q, \Omega), \tag{35}$$

$$q'' + \eta_{02}^2 q = \varepsilon\tilde{f}_{\mathrm{NL},2}(p, q, \Omega). \tag{36}$$

Equations 35 and 36 describe the equations of motion of the system in the modal coordinates. The equations are weakly coupled because the terms on the right side of the equation are of the order ε. In order to obtain decoupled equations, only the corresponding modal coordinate is considered exclusively near its resonant frequency. Therefore the remaining modal coordinate is neglected [4]. This leads to the decoupled equations of motion in the modal coordinates

$$\eta \approx \eta_{01}:\ p'' + \eta_{01}^2 p = \varepsilon\tilde{f}_{\mathrm{NL},1}(p, 0, \Omega), \tag{37}$$

$$\eta \approx \eta_{02}:\ q'' + \eta_{02}^2 q = \varepsilon\tilde{f}_{\mathrm{NL},2}(0, q, \Omega). \tag{38}$$

In order to derive an analytical solution, a Van der Pol transformation is applied to the system analogous to the lock-up damper and the slowly changing amplitude and phase differences of the system are investigated

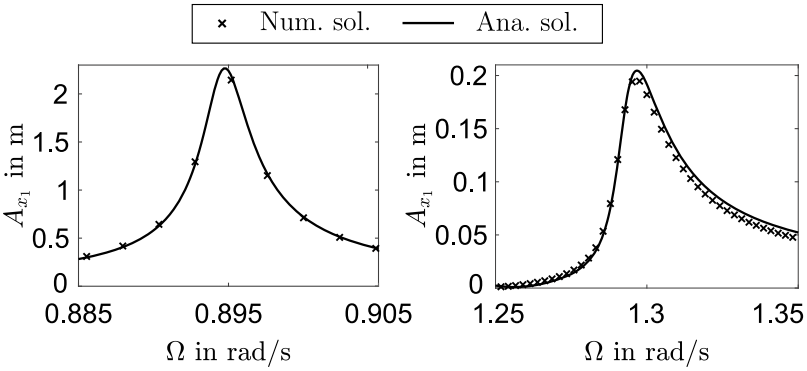

Fig. 10 Analytical solution of the prestressed sliding wedge damper for the standard parameters

$$p = A_1 \sin\varphi_1,\ p' = A_1\eta_{01}\cos\varphi_1,\ \varphi_1 = \eta\tau + \psi_1, \tag{39}$$

$$q = A_2 \sin\varphi_2,\ q' = A_2\eta_{02}\cos\varphi_2,\ \varphi_2 = \eta\tau + \psi_2, \tag{40}$$

$$i = \{1, 2\},\ \delta_i = \eta_{0i} - \eta, \tag{41}$$

$$A_i' = \varepsilon\, \tilde{f}_{\mathrm{NL,i}}(A_i, \psi_i, \varphi_i)\cos\varphi_i, \tag{42}$$

$$\psi_i' = \varepsilon\left(\delta_i - \frac{1}{A_i\eta_{0i}}\tilde{f}_{\mathrm{NL,i}}(A_i, \psi_i, \varphi_i)\cos\varphi_i\right). \tag{43}$$

The stationary solution of the equations for A_i and ψ_i is determined by the averaging procedure and the results are shown in Fig. 10. It can be seen that the analytical solution approximates the numerical results with the accuracy of asymptotic methods. The deviations from the numerical solution are of the order ε, which confirms the validity of the analytic solution.

4 The Friction Damper with Polynomial Contact Geometries

The friction damper with polynomial contact geometries is quite similar to the sliding wedge damper analyzed in Sect. 3. The damper is attached to the main system and is composed of two main elements: a vibration absorber and two contact surfaces with a polynomial geometry. The secondary spring c_2 and secondary mass m_2 make up the absorber portion of the damper and allow it to reduce vibration in the vicinity of the tuned frequency. As with the sliding wedge damper, the contact surfaces are clamped on to the secondary mass via a third spring c_3 and the prestress displacement $\Delta\ell$. The geometry of the contact surfaces are described by the function $y(x_{\mathrm{rel}}) = y(x_2 - x_1) = \gamma|x_2 - x_1|^n$ with $n \in \mathbb{N}$. For the sake of simplicity only one polynomial term is introduced in the function y. Additionally, the coefficient μ describes the

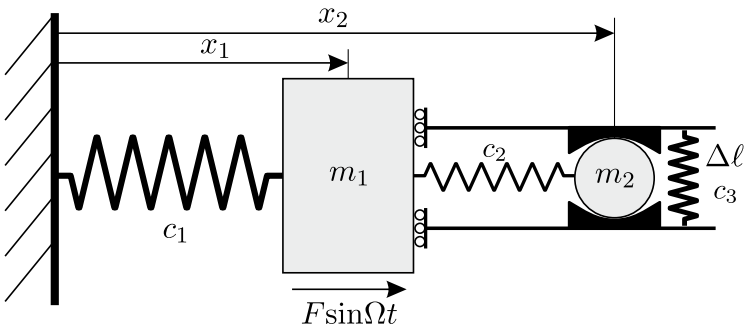

Fig. 11 The friction damper with polynomial contact geometry

relationship between the normal force and the friction force acting on the secondary mass (or on the contact surfaces) (Fig. 11).

As with the sliding wedge damper, the prestress level determines when the system finds itself in the linear sticking range or in the nonlinear stick-slip range. The equations of motion for both ranges are given by

while sticking

$$(m_1 + m_2)\ddot{x}_1 + c_1 x_1 = F \sin \Omega t, \tag{44}$$

$$H = \frac{m_2}{m_1 + m_2}(F \sin \Omega t - c_1 x_1), \tag{45}$$

while sliding

$$m_1\ddot{x}_1 + c_1 x_1 - c_2(x_2 - x_1) - F_{PD} = F \sin \Omega t, \tag{46}$$

$$m_2\ddot{x}_2 + c_2(x_2 - x_1) + F_{PD} = 0, \tag{47}$$

$$F_{PD} = 2c_3(2y + \Delta\ell)\frac{y_x + \mu \mathrm{sgn}(\dot{x}_2 - \dot{x}_1)}{1 - \mu \mathrm{sgn}(\dot{x}_2 - \dot{x}_1) y_x}, \tag{48}$$

$$y = \gamma |x_2 - x_1|^n, \quad y_x = n\gamma |x_2 - x_1|^{n-1} \mathrm{sgn}(x_2 - x_1). \tag{49}$$

Analogous to the sliding wedge damper, the force F_{PD} is linearized with respect to the friction coefficient. This linearization allows an insight into the damper force and a practicable separation into a dissipation free $F_{\mathrm{C,PD}}$ and dissipativ portion $F_{\mathrm{D,PD}}$. These quantities are given by

$$F_{\mathrm{PD}} \approx F_{\mathrm{PD,lin}} = F_{\mathrm{C,PD}} + F_{\mathrm{D,PD}}, \tag{50}$$

$$F_{\mathrm{C,PD}} = 4c_3\gamma^2 n(x_2 - x_1)^{2n-1} + 2c_3\Delta\ell\gamma n|x_2 - x_1|^{n-1}\mathrm{sgn}(x_2 - x_1), \tag{51}$$

$$\begin{aligned} F_{\mathrm{D,PD}} = {} & 4c_3\mu\left(\gamma|x_2 - x_1|^n + \gamma^3 n^2 |x_2 - x_1|^{3n-2}\right)\mathrm{sgn}(\dot{x}_2 - \dot{x}_1) \\ & + 2c_3\Delta\ell\mu\left(1 + \gamma^2 n^2 |x_2 - x_1|^{2n-2}\right)\mathrm{sgn}(\dot{x}_2 - \dot{x}_1). \end{aligned} \tag{52}$$

As noticed from Eqs. 51 and 52, the contact geometries introduce a dominant nonlinear stiffness of the degree $2n - 1$, as well as a dominant nonlinear damping of the

degree $3n-2$. These terms will mainly determine the behavior of the systems in the resonance regimes and the damping capability of the system.

Since the analytical procedure was validated for the sliding wedge damper, the investigations in this section are limited to analytical considerations of the friction damper with polynomial contact geometries. To this end, the equations of motion are nondimensionalized. In order to ensure a vibration absorption frequency, dominant linear terms are required for low amplitude vibrations. Therefore, a soft spring c_3 is chosen with $c_3 = \varepsilon \tilde{c}_3$ and $\varepsilon \ll 1$. The necessary transformations for the analytical considerations are given by

$$\frac{m_2}{m_1} = \lambda,\ \frac{c_1}{m_1} = \omega_{01}^2,\ \tau = \omega_{01} t,\ \frac{\mathrm{d}(\ )}{\mathrm{d}t} = \omega_{01}\frac{\mathrm{d}(\ )}{\mathrm{d}\tau},\ \eta = \frac{\Omega}{\omega_{01}},\ p = \frac{c_2}{m_1\omega_{01}}, \tag{53}$$

$$a = \frac{4\tilde{c}_3}{m_1\omega_{01}^2},\ b = \frac{4\tilde{c}_3\mu}{m_1\omega_{01}^2},\ c = \frac{2\tilde{c}_3\Delta\ell}{m_1\omega_{01}^2},\ d = \frac{2\tilde{c}_3\Delta\ell\mu}{m_1\omega_{01}^2},\ \varepsilon f = \frac{F}{m_1\omega_{01}^2}. \tag{54}$$

Inserting these transformations in the equations of motion yields

$$x_1'' + x_1 - p^2(x_2 - x_1) = \varepsilon(f\sin\eta\tau + f_{\mathrm{PD}}) = \varepsilon f_1, \tag{55}$$

$$\lambda x_2'' + p^2(x_2 - x_1) = -\varepsilon f_{\mathrm{PD}} = \varepsilon f_2, \tag{56}$$

$$\begin{aligned} f_{\mathrm{PD}} = {} & a\gamma^2 n(x_2 - x_1)^{2n-1} + b\left(\gamma|x_2 - x_1|^n + \gamma^3 n^2|x_2 - x_1|^{3n-2}\right)\mathrm{sgn}(x_2' - x_1') \\ & + c\gamma n|x_2 - x_1|^{n-1}\mathrm{sgn}(x_2 - x_1) + d\left(1 + \gamma^2 n^2|x_2 - x_1|^{2n-2}\right)\mathrm{sgn}(x_2' - x_1')\,. \end{aligned} \tag{57}$$

Subsequently, a modal coordinate transformation is applied yielding first the weakly coupled differential equations in the modal coordinates. By only considering the corresponding modal coordinate in the respective resonance regime, the fully decoupled differential equations are obtained

$$\eta \approx \eta_{01}:\ p'' + \eta_{01}^2 p = \varepsilon(r_{11} f_1(p, 0) + r_{21} f_2(p, 0)), \tag{58}$$

$$\eta \approx \eta_{02}:\ q'' + \eta_{02}^2 q = \varepsilon(r_{12} f_1(0, q) + r_{22} f_2(0, q)). \tag{59}$$

For the sake of brevity and due to the length of the expressions further equations are omitted. The parameters are chosen as follows

$$m_1 = 1,\ m_2 = 0.1,\ c_1 = 1,\ c_2 = 0.1,\ c_3 = 0.01,$$
$$\Delta\ell = 0.1,\ \gamma = 1,\ \mu = 0.1,\ F = 0.01.$$

The first consideration focuses on the amplitude response of the polynomial damper for different polynomial degrees, c.f. Fig 12. As expected, multiple solution branches exist for $n > 1$ due to the nonlinear stiffness terms. Here the advantages and disadvantages of the damper are noted. Due to the nonlinear dissipative terms the maximal amplitude of the system is greatly reduced. For example a polynomial degree of $n = 4$ leads to a maximum amplitude reduction of 72, 9% in comparison to a polynomial contact surface with $n = 1$. This amplitude reduction comes at the price of multiple branch solutions, thus leading to higher possible amplitudes within the multiple

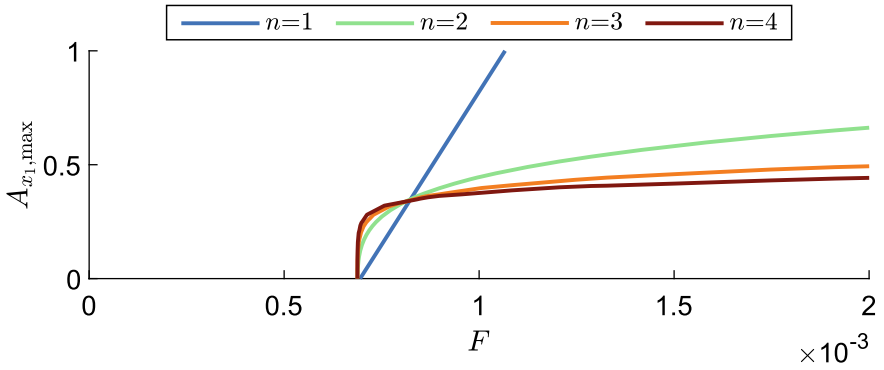

Fig. 12 Amplitude response of the friction damper with polynomial contact geometries for different polynomial degrees

solution range and amplitude jump when leaving said range. Especially the jumps in amplitude could prove detrimental to the function and life span of the main system [3]. Furthermore, the multiple solution range increases with the excitation leading to an amplitude rise over a wider range. However, if the excitation amplitude is known and a system overload can be excluded, the polynomial contact surface can be designed in order to avoid multiple solutions and effectively reduce amplitude vibrations.

An additional analytical consideration evaluates the relationship between the excitation force and the maximal amplitude in the system's response. Figure 13 shows that for low excitation forces the contact surface with lower polynomial degree result in lower maximal amplitudes. This is due to the relationship between the dissipated energy and the relative displacement, which is approximately described by $E_D \sim (A_{\text{rel}}/K)^{3n-1}$. As is seen from this relationship, low values of A_{rel} caused by

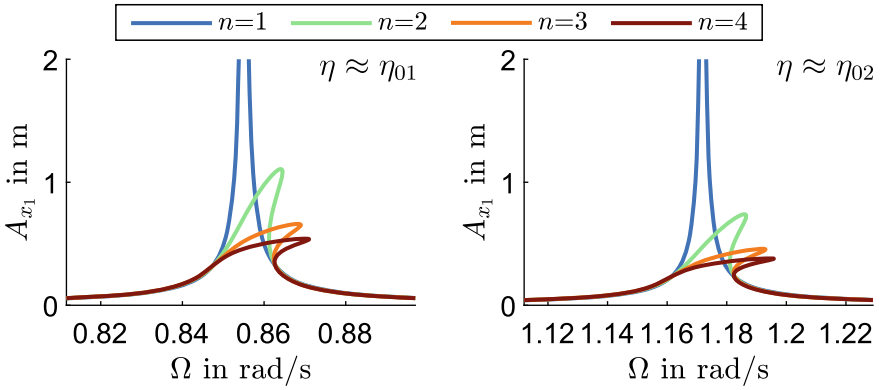

Fig. 13 Excitation vs maximal amplitude relationship for different polynomial degrees

low excitation forces lead to a significantly lower dissipated energy for $n > 1$. Furthermore, all curves cross the same point where the exponent has no influence on the dissipated energy, c.f. Fig 12.

5 Experiments

Based on the described analytic results, an experimental setup has been developed. The first experiments were performed together with the group of Professor Sattel at the TU Ilmenau, see Fig. 14. This setup allows for the investigation of different add-on damper systems at comparatively low frequencies (10–60 Hz) with large amplitudes (0.1–2 mm). The results confirm the theoretically predicted behavior, c.f. Figs. 2, 3 and 15. In Fig. 15a, the curves represent different preloads of the friction contact. The blue curves correspond to a zero breakaway force (no preload). The system behaves as a tuned mass damper, demonstrating two prominent peaks and the strong suppression of vibrations at the tuning frequency. The red curves correspond to very high preload, which ensures permanent sticking in the friction contact. The system's behavior in the last case corresponds to a one degree of freedom oscillator. The curves in between demonstrate that the lock-up damper is able to damp the peak around the first resonance. Furthermore, the systems sensitivity with respect to the excitation amplitude was also validated, c.f. Fig 15b. A comparison between the dry friction lock-up damper and a magneto-electro rheological damper is presented in [12].

In order to validate the numerical and analytical predictions of the performance of the wedge damper, a second setup was designed, see Fig. 16. To a certain extent, this setup uses the same parts as the setup for the lock-up damper and is also designed for low frequencies and large amplitudes. The experimental results confirm the numerical and analytical simulations. The prestress level on the damper determined how the

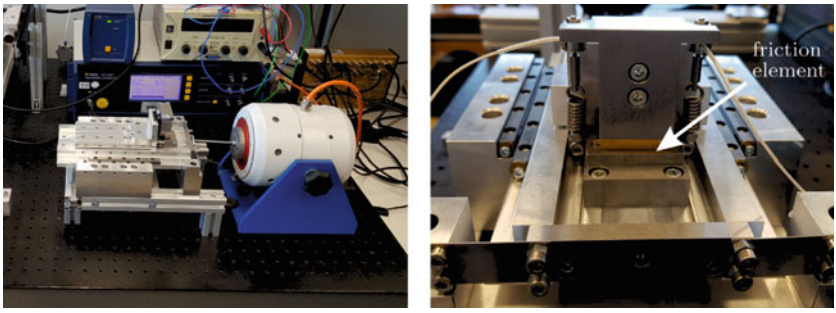

a) b)

Fig. 14 **a** Experimental setup for testing of the lock-up mass damper. **b** Detailed view on the lock-up element

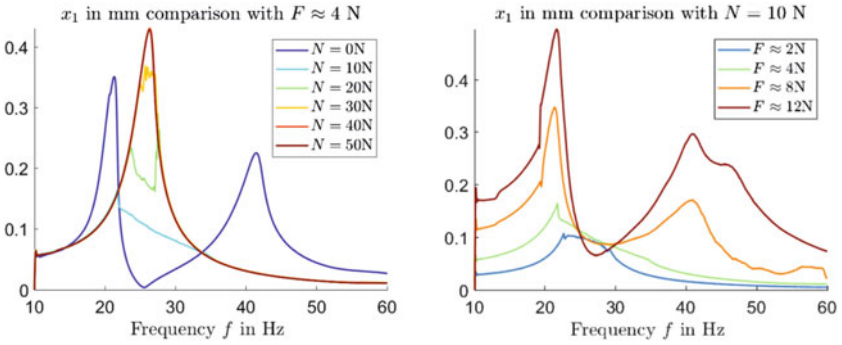

Fig. 15 **a** Prestress variation results. **b** Excitation amplitude variation results

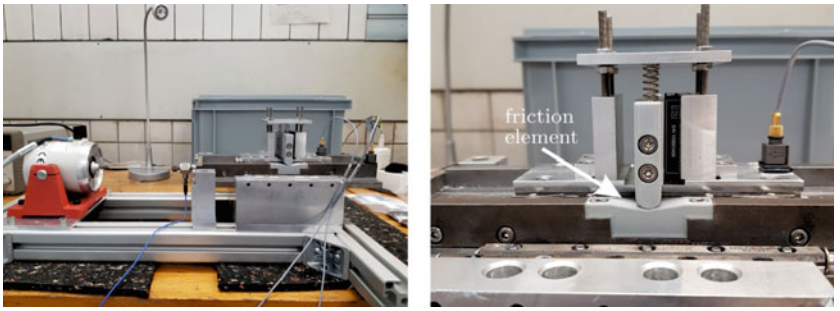

Fig. 16 **a** Experimental setup for testing of the wedge damper. **b** Detailed view on the wedge element

system behaves, analogously to the breakaway force of the lock-up damper. If the prestress level is too high, the system behaves as a one degree of freedom system, whereas if it is set to zero, a system with two degrees of freedom is observed, c.f. Fig. 16a. Additionally, Fig. 16b shows the magnification factor V for different excitations amplitudes and proves the damper's robustness, i.e. its scalability (Fig. 17).

6 Conclusions

This work investigated three friction based dampers: the lock-up damper, the sliding wedge damper, and the friction damper with polynomial contact surfaces. It can be stated that the friction-based dampers demonstrate their ability to diminish forced vibrations tightly focused on the resonance ranges. Furthermore, the contact geometry significantly determines the characteristics of the damper. The planar contact

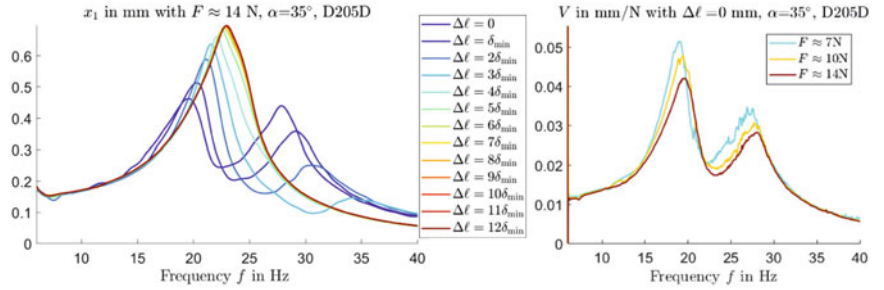

Fig. 17 **a** Prestress variation results $6\delta_{\min} = 0.7$ mm. **b** Magnification factor results for different excitation amplitudes

geometry of the dry lock-up damper has a limited robustness and therefore a reduced applicability. An increase in robustness is observed in the prestressed wedge damper, which has a linear varying contact geometry. In order to avoid unnecessary energy losses, the wedge damper can be prestressed and forced into the stick-phase as long as the vibrations remain sufficiently small. These passive dampers are either optimal in the passage through resonance or at a certain tuned frequency, but not in both. The friction based damper with polynomial contact surfaces addresses this limited applicability to a certain extent. Namely, when the range of the excitation force amplitude is known a priori.

The developed analytical approaches enable to predict the behavior of such systems and to make the reasonable parameter choice for the design of real devices. These analytical results are verified via experiments for the lock-up damper and the sliding wedge damper. Comparing the analytical results, it is noted that the developed approach based on the averaging technique enables accurate prediction of the dynamics of such devices.

Acknowledgements The authors would like to express their gratitude towards the German Research Foundation, Deutsche Forschungsgemeinschaft (DFG) for the financial support within the priority program SPP 1897, 'Calm, Smooth, and Smart - Novel Approaches for Influencing Vibrations by Means of Deliberately Introduced Dissipation'.

References

1. Den Hartog, J.P.: Mechanical Vibrations. Dover Publications, New York (1985)
2. Dixon, J.C.: The Shock Absorber Handbook. Wiley, New York (2008)
3. Dresig, H., Fidlin, A.: Schwingungen mechanischer Antriebssysteme. Springer, Berlin (2006)
4. Fidlin, A., Gafur, N.: On the dynamics of friction based tuned mass dampers. In: Proceedings of ENOC the 9th EUROMECH Nonlinear Dynamics Conference (2017)
5. Fidlin, A., Lobos, M.: On the limiting of vibration amplitudes by a sequential friction-spring element. J. Sound Vib. **333**(23), 5970–5979 (2014)

6. Fidlin, A., Aramendiz, J.: Study on the dynamics of a lockup mass damper: asymptotic analysis and application limits. Nonlinear Dyn. **97**, 1867–1875 (2018)
7. Fleischer, G., Wachter, K.: Konstruktionslehre für Maschineningenieure. Verl. Technik, Berlin (1987)
8. Hausner, M., Hässler, M.: Kupplungsscheibe mit frequenztilger gegen rupfschwingungen. ATZ-Automobiltechnische Zeitschrift **114**(1), 64–69 (2012)
9. Khoo, H.H., Clifton, C., Butterworth, J., MacRae, G., Gledhill, S., Sidwell, G.: Development of the self-centering Sliding Hinge Joint with friction ring springs. J. Constr. Steel Res. **78**, 201–211 (2012)
10. Panning, L.; Sextro W.; Popp K.: Optimization of interblade friction damper design. In: Proceedings of the ASME Turbo Expo 2000: Power for Land, Sea, and Air (2000)
11. Sun, J., Jolly, M.R., Norris, M.: Passive, adaptive and active tuned vibration absorbers-a survey. J. Mech. Design **117**(B), 234–242 (1995)
12. Tan, A.S., Aramendiz, J., Ross, K.H., Sattel, T., Fidlin, A.: Comparative study between dry friction and electrorheological fluid switches for tuned vibration absorbers. J. Sound Vibrat. 114874 (2019)
13. Weber, F., Høgsberg, J., Krenk, S.: Optimal tuning of amplitude proportional Coulomb friction damper for maximum cable damping. J. Struct. Eng. **136**(2), 123–134 (2002)
14. Wu, Q., Cole, C., Spiryagin, M., Sun, Y.Q.: A review of dynamics modelling of friction wedge suspensions. Veh. Syst. Dyn. **52**(11), 1389–1415 (2014)